Video Article

Synthesis and Characterization of Fe-doped Aluminosilicate Nanotubes with Enhanced Electron Conductive Properties

Ehsan Shafia[1], Serena Esposito[2], Elnaz Bahadori[1], Marco Armandi[1,3], Maela Manzoli[4], Barbara Bonelli[1,3,5]

[1]Department of Applied Science and Technology, Politecnico di Torino

[2]Department of Civil and Mechanical Engineering, Università degli Studi di Cassino e del Lazio Meridionale

[3]Institute of Chemistry, Politecnico di Torino

[4]Department of Chemistry & NIS Interdepartmental Centre, University of Turin

[5]INSTM Unit of Torino-Politecnico, Politecnico di Torino

Correspondence to: Barbara Bonelli at barbara.bonelli@polito.it

URL: https://www.jove.com/video/54758
DOI: doi:10.3791/54758

Keywords: Chemistry, Issue 117, nanotubes, Fe-doping, band gap lowering, sol-gel synthesis, nanomaterials characterization, imogolite, aluminosilicate, azo-dyes, adsorption, ζ-potential, Fe_2O_3 clusters, isomorphic substitution

Date Published: 11/15/2016

Citation: Shafia, E., Esposito, S., Bahadori, E., Armandi, M., Manzoli, M., Bonelli, B. Synthesis and Characterization of Fe-doped Aluminosilicate Nanotubes with Enhanced Electron Conductive Properties. *J. Vis. Exp.* (117), e54758, doi:10.3791/54758 (2016).

Abstract

The goal of the protocol is to synthesize Fe-doped aluminosilicate nanotubes of the imogolite type with the formula $(OH)_3Al_{2-x}Fe_xO_3SiOH$. Doping with Fe aims at lowering the band gap of imogolite, an insulator with the chemical formula $(OH)_3Al_2O_3SiOH$, and at modifying its adsorption properties towards azo-dyes, an important class of organic pollutants of both wastewater and groundwater.

Fe-doped nanotubes are obtained in two ways: by direct synthesis, where $FeCl_3$ is added to an aqueous mixture of the Si and Al precursors, and by post-synthesis loading, where preformed nanotubes are put in contact with a $FeCl_3 \cdot 6H_2O$ aqueous solution. In both synthesis methods, isomorphic substitution of Al^{3+} by Fe^{3+} occurs, preserving the nanotube structure. Isomorphic substitution is indeed limited to a mass fraction of ~1.0% Fe, since at a higher Fe content (*i.e.,* a mass fraction of 1.4% Fe), Fe_2O_3 clusters form, especially when the loading procedure is adopted. The physicochemical properties of the materials are studied by means of X-ray powder diffraction (XRD), N_2 sorption isotherms at -196 °C, high resolution transmission electron microscopy (HRTEM), diffuse reflectance (DR) UV-Vis spectroscopy, and ζ-potential measurements. The most relevant result is the possibility to replace Al^{3+} ions (located on the outer surface of the nanotubes) by post-synthesis loading on preformed imogolite without perturbing the delicate hydrolysis equilibria occurring during nanotube formation. During the loading procedure, an anionic exchange occurs, where Al^{3+} ions on the outer surface of the nanotubes are replaced by Fe^{3+} ions. In Fe-doped aluminosilicate nanotubes, isomorphic substitution of Al^{3+} by Fe^{3+} is found to affect the band gap of doped imogolite. Nonetheless, Fe^{3+} sites on the outer surface of nanotubes are able to coordinate organic moieties, like the azo-dye Acid Orange 7, through a ligand-displacement mechanism occurring in an aqueous solution.

Video Link

The video component of this article can be found at https://www.jove.com/video/54758/

Introduction

The term nanotube (NT) is universally associated with carbon nanotubes[1], one of the most-studied chemical objects today. Less known is the fact that aluminosilicate NTs can also be synthesized[2,3], in addition to being present in nature (mainly in volcanic soils). Imogolite (IMO) is a hydrated aluminosilicate with the formula $(OH)_3Al_2O_3SiOH$[4,5], occurring as single-walled NT with Al(OH)Al and Al-O-Al groups on the outer surface and non-interacting silanols (SiOH) on the inner one[6]. Concerning geometry, the length varies from a few nm to several hundred nm[3,5,7]. The inner diameter is constant at 1.0 nm[5], whereas the outer diameter is ~2.0 nm in natural IMO, increasing to 2.5-2.7 nm in samples synthetized at 100 °C. Synthesis at 25 °C yields NTs with outer diameters close to that of natural IMO instead[8]. Recently, it has been shown that NTs with different external diameters may also be obtained by changing the acid used during the synthesis[9]. In the dry powder, IMO NTs assemble in bundles with nearly hexagonal packing (**Figure 1**). Such an array of NTs gives rise to three kinds of pores[10,11] and related surfaces[12]. Besides proper intra-tube A pores (1.0 nm in diameter), smaller B pores (0.3-0.4 nm wide) occur among three aligned NTs within a bundle, and, finally, larger C pores occur as slit-mesopores among bundles (**Figure 1**). Both chemical composition and pore dimension affect the adsorption properties of the material. The surfaces of A pores are very hydrophilic, as they are lined with SiOH, and are able to interact with vapors and gases like H_2O, NH_3, and CO[12]. Because they are small, B pores are hardly accessible, even to small molecules like water[10,11], whereas C pores may interact with larger molecules like phenol[6] and 1,3,5-triethylbenzene[12]. Amara *et al.* have recently shown that hexagonalization of NTs organized in closely-packed bundles occurs with (imogolite analogue) aluminogermate NTs[13]. This phenomenon, though not observed so far with aluminosilicate NTs, could affect the accessibility of B pores as well.

Interest in IMO-related chemistry has increased recently, partly due to the possibility of changing the composition of both the inner and the outer surface of NTs. The presence of a plethora of hydroxyls renders IMO extremely sensitive to thermal degradation, since dehydroxylation occurs above 300 °C[6,14-16] with consequent NT collapse.

The inner surface may be modified by several methods, including the substitution of Si atoms with Ge atoms[17], which causes the formation of either single- or double-walled[18] NTs with the formula $(OH)_3Al_2O_3Si_{1-x}Ge_xOH$[19]. Post-synthesis grafting of organic functionalities leads to the formation of NTs with the formula $(OH)_3Al_2O_3SiO$-R, where R is the organic radical[20]. Through one-pot synthesis in the presence of a Si precursor containing one organic radical directly linked to the Si atom, formation hybrid NTs form, with the formula $(OH)_3Al_2O_3Si$-R (R = $-CH_3$, $-(CH_2)_3-NH_2$)[21,22].

Modification of the outer surface is of the utmost interest for the fabrication of imogolite/polymer composites[23] and involves either electrostatic interactions or covalent bonding. The former method is based on the charge matching between the outer surfaces of the NTs and a proper counter-ion (*e.g.,* octadecylphosphonate)[24,25]; the latter method implies a reaction between pre-formed IMO NTs and an organosilane (*e.g.,* 3-aminopropylsilane)[26].

In water, electrostatic interactions between IMO and ions are possible due to the following equilibria[27]

$Al(OH)Al + H^+ = Al(OH_2)^+Al$ (1)

$SiOH = SiO^- + H^+$ (2)

leading to charged surfaces that have been tested in anion/cation retention from polluted water[28-32].

The present work concerns yet another modification of the outer surface (*i.e.,* the isomorphic substitution of (octahedral) Al^{3+} with Fe^{3+}, hereafter referred to as Al^{3+}/Fe^{3+} IS). This phenomenon is indeed common in minerals, whereas less is known about Al^{3+}/Fe^{3+} IS in IMO NTs.

Concerning doping, the first issue is the total amount of iron that can be hosted by the NTs without causing severe structural strains. A pioneering experimental work on Fe-doped IMO showed that NTs do not form at Fe mass fractions higher than 1.4%[33]. Successive theoretical calculations showed that Fe could either isomorphically substitute for Al or create "defective sites"[34]. Such defects (*i.e.,* iron oxo-hydroxide clusters) were supposed to reduce the band gap of IMO (an electrical insulator)[34,35] from 4.7 eV to 2.0-1.4 eV[34]. Accordingly, we have recently shown that the presence of Fe^{3+} imparts the solid with new chemical and solid-state properties, lowering the band gap of IMO (E_g = 4.9 eV) to 2.4-2.8 eV[36].

A recent report on Fe-doped aluminum-germanate NTs, isostructural with IMO, showed that actual Al^{3+}/Fe^{3+} IS is limited to a mass fraction of 1.0% Fe, since the formation of iron oxo-hydroxide particles unavoidably occurs at a higher Fe content due to the natural tendency of Fe to form aggregates[37]. Similar results were obtained with Fe-doped IMO NTs[33,36,38-40].

From a scientific point of view, the determination of the state of Fe and of its possible reactivity and adsorption properties in Fe-doped IMO is an important issue that requires several characterization techniques.

In this work, we report the synthesis and characterization of Fe-doped IMO. Two samples were synthesized with a mass fraction of 1.4% Fe by either direct synthesis (Fe-x-IMO) or post-synthesis loading (Fe-L-IMO); a third sample with a lower iron content (corresponding to a mass fraction of 0.70%) was obtained through direct synthesis in order to avoid cluster formation and to obtain a material in which mostly Al^{3+}/Fe^{3+} IS occurred. In this case, the formation of NTs with the chemical formula $(OH)_3Al_{1.975}Fe_{0.025}O_3SiOH$ is expected. Morphological and textural properties of the three Fe-doped IMO are compared to those of proper IMO. In addition, surface properties related to Fe(OH)Al groups are studied in water by measuring the ζ potential and the interaction with the (bulky) anion of the azo-dye Acid Orange 7 (NaAO7), a model molecule of azo-dyes, which are an important class of pollutants of both wastewater and groundwater[41]. $AO7^-$ structure and molecular dimensions are reported in **Figure 2a**, along with the UV-Vis spectrum (**Figure 2b**) of a 0.67 mM water solution (natural pH = 6.8). Due to its molecular dimensions[42], the $AO7^-$ species should mainly interact with the outer surface of NTs, limiting parasitic interactions possibly deriving from diffusion within IMO inner pores, so it can be used as a probe molecule of the outer surface.

Protocol

1. Synthesis of 3 g of IMO NTs

1. In a dry room, prepare an 80 mM $HClO_4$ solution by slowly adding 1.3 ml of perchloric acid with a mass fraction of 70% to 187.7 ml of double-distilled water at room temperature (r.t.). Use a 2,000-ml beaker that will be useful for successive dilutions (step 1.6).
2. In a smaller beaker in the dry room, mix 8 ml of aluminum-tri-*sec*-butoxide (97%) (ATSB; the source of aluminum)[43,44] and 3.8 ml of tetraethyl orthosilicate (98%) (TEOS; the source of Si) in the molar ratio Al:Si = 2:1.1. Use graduated pipettes to measure the volumes of reagents.
3. Leave the mixture under mild stirring for one min until a clear and uniform mixture (without any suspended solid particles) is obtained.
4. Immediately after, with a Pasteur pipette, dropwise add the whole mixture to the aqueous solution of $HClO_4$ under stirring (the final molar ratios are Si:Al:$HClO_4$ = 1.1:2:1). By adding the mixture to the $HClO_4$ aqueous solution, white clusters form and the pH increases to 5.
5. Stir the final mixture at r.t. for about 18 hr, until a transparent solution is obtained.
6. Under stirring, add 1.3 L of double-distilled water (measured with a graduated cylinder) to dilute the solution to 20 mM with respect to Al. Stir the obtained 20 mM Al solution for about 20 min.
7. Pour the mixture into a polytetrafluoroethylene autoclave (with thick walls) and leave it within a stove for 4 d at 100 °C without stirring.
8. After 4 d, filter the clear and transparent solution (use a 0.02 micron filter) to collect the NTs and wash with double-distilled water, obtaining a dense, transparent mixture.
9. Dry the mixture in a stove at 50-60 °C for 1 d. The final IMO powder has a white color.

2. Synthesis of 3 g Fe-x-IMO NTs (with a mass fraction of either 0.70% or 1.4% Fe)

1. In a dry room, prepare an 80 mM solution of $HClO_4$ by slowly adding 1.3 ml of perchloric acid with a mass fraction of 70% to 187.7 ml of double-distilled water (pH = 1.0). Use a 2,000-ml beaker that will be useful for successive dilutions (step 2.6).
2. Dissolve 0.1 g of $FeCl_3$•$6H_2O$ in the $HClO_4$ acid solution to obtain Fe-0.70-IMO NTs.
3. Dropwise add 8 ml of ATSB and 3.8 ml of TEOS into the iron-containing solution. Use graduated pipettes to measure reagent volumes. Check that the pH is equal to 4. Leave the mixture under stirring at r.t. for 18 hr.
4. After 18 hr, dilute the resulting solution to 20 mM in Al by adding 1.3 L of double-distilled water (measured with a graduated cylinder) and maintain it under stirring for 1 hr. Afterwards, pour it inside a sealed polytetrafluoroethylene autoclave (with thick walls) and leave it within a stove for 4 d at 100 °C.
5. Filter the solution, wash the resulting reddish-brown powder with double-distilled water, and dry it overnight at 50 °C in an oven.
6. In order to prepare Fe-1.4-IMO NTs, repeat all the steps with 0.2 g of $FeCl_3$•$6H_2O$.

3. Synthesis of Fe-L-IMO NTs

1. Disperse 0.25 g IMO in 15 ml of double-distilled water.
2. Add 0.025 g $FeCl_3$•$6H_2O$ to the mixture (weight calculated considering a slight excess of iron(III) chloride hexahydrate). Leave under stirring for 18 hr; after 18 hr of stirring, the color of the mixture turns from yellow to reddish-brown, indicating the initial formation of iron oxo/hydroxide species.
3. Add 3.0 ml of water and 1.5 ml of NH_4OH solution (mass fraction of 33%) to precipitate all Fe^{3+} species as oxo/hydroxide.
4. Filter the mixture, wash the resulting powder with double-distilled water, and dry it in a stove at 120 °C for 48 hr.

4. Sample Characterization

1. Before measuring low-angle X-ray diffraction (XRD) patterns of the sample, mill 100 mg of the powder in an agate mortar, deposit it on a sample holder, and press it with care in order to get a uniform and smooth surface. Instrumental parameters of XRD patterns reported here are detailed in Ref. 36.
2. To obtain high resolution electron transmission microscopy (HRTEM) micrographs, mill 10 mg of powder in an agate mortar. In order to obtain a well-dispersed sample for HRTEM inspection, put the milled powder in contact with a Cu grid covered with a Lacey carbon film.
    1. Remove the excess by gently shaking the grid in order to leave only a few grains electrostatically interacting with the sample holder. Avoid dispersing the powder in a solvent, which could modify the NT arrangement. Instrumental parameters of HRTEM measurements reported here are detailed in Ref. 36 and 39.
3. To determine the BET SSA (Brunauer-Emmett-Teller Specific Surface Area) and porous volume values reported in **Table 1**, measure N_2 adsorption/desorption isotherms at -196 °C. Before measurement, outgas the samples at 250 °C in order to remove water and other atmospheric contaminants[10] while still preserving NTs[6,14-16]. The instrumental details are reported in Ref. 39.
4. Outgas the powder in a UV-Vis quartz cell connected to a standard vacuum frame (residual pressure below 10^{-3} mbar) and take its diffuse reflectance (DR) UV-Vis spectrum. The instrumental parameters of DR-UV-Vis spectra reported here are detailed in Ref. 36.
   NOTE: Experimental and instrumental details concerning electrophoretic mobility measurements are reported in Ref. 39.
5. NaAO7 adsorption experiments
    1. Prepare 200 ml of 0.67 mM NaAO7 solution by adding double-distilled water to 0.047 g NaAO7 in a volumetric flask. The solution pH should be 6.80.
    2. Pour 50 ml of the solution inside a dark bottle and add 50 mg of IMO (powder concentration 1 g/L). Keep the solution under stirring during the experiment. Repeat this step with the other powders (powder concentration 1 g/L).
    3. At regular time intervals (t: 0 sec, 5 min, 10 min, 45 min, 2 hr, 5 hr, 24 hr, and 72 hr), recover 5 ml of the supernatant by centrifugation at 835 x g for 3 min.
    4. Analyze the supernatant by transmission UV-Vis spectroscopy in a 1-mm path cuvette. In water, $AO7^-$ undergoes azo-hydrazone tautomerism, whereas the hydrazone form is stable in the solid phase, as shown by the UV-Vis spectrum in **Figure 2b**. Determine the amount of $AO7^-$ removed from the solution by measuring the decrease of the 484 nm band intensity of the hydrazone form, according to the literature[38,39,41].

Representative Results

Concerning the synthesis of IMO and Fe-doped IMO NTs, the most relevant issues are i) the formation of NTs, especially during Fe-doping by direct synthesis; ii) the actual environment of Fe species in the final materials; and iii) the effect of Fe on the physicochemical properties of the material, especially its band gap and its adsorption properties. The presence of Fe at the outer surface of NTs is indeed expected to modify the interactions between the NTs and the adsorbate species, especially in water solutions. The above aspects have to be assessed by multiple characterization techniques. DR-UV-Vis spectroscopy is used to assess the coordination of iron species in doped samples, as well as the presence of isolated Fe^{3+} sites and/or iron oxo-hydroxide clusters. ζ-potential measurements allow studies of the surface charge of the samples in an aqueous environment and adsorption of $AO7^-$ to assess the behavior of the material towards an azo-dye used to probe the NT external surface.

The successful synthesis of NTs is documented by XRD patterns and HRTEM analyses. All the samples showed the typical XRD pattern ascribable to NTs organized in a hexagonal array (**Figure 3a**)[43]. The main peak corresponds to the d_{100} reflection, from which the cell parameter, which corresponds to the center-to-center distance between two aligned NTs in a hexagonal packing (**Figure 1**), is calculated as $a = 2d_{100}/\sqrt{3}$. The d_{100} peak is in the same position ($2\Theta = 3.88°$) with both IMO and Fe-L-IMO, whereas it shifts to slightly higher angles with samples prepared by direct synthesis, leading to a decrease in the corresponding values of both d_{100} and *a*. This phenomenon was ascribed to the replacement of (bulkier) ClO_4^- ions, present in the synthesis batch of IMO[16], by (smaller) Cl^- ions deriving from the Fe precursor, with a consequent decrease of the interspace between adjacent NTs[39]. Formation of NTs is confirmed by HRTEM analysis; the reported micrographs concerning the Fe-0.70-IMO sample show a bundle of NTs (**Figure 3b**) in a hexagonal array (**Figure 3c**). N_2 isotherms (not reported) allowed for the measurement of BET SSA and pore volumes (**Table 1**). As a whole, the presence of Fe leads to an increase in surface area. The sample obtained by loading has a larger total volume; the difference with respect to micropore volume, mainly related to A pores, indicates that the loading procedure mainly affected the outer surface of NTs.

The state of Fe is studied by means of DR-UV-Vis spectra in **Figure 4a**. Similar curves are seen for the Fe-containing samples, whereas IMO (a white powder) weakly absorbs in the UV-Vis range. Both Fe-0.70-IMO and Fe-1.4-IMO mainly absorb at 270 nm; a minor absorption at 480 nm is clearly visible with Fe-1.4-IMO, but it is almost negligible with Fe-0.70-IMO. Such results indicate the occurrence of Al^{3+}/Fe^{3+} IS with both samples, since the band at 270 nm is due to charge-transfer transitions (CT) from O^{2-} to isolated octahedral Fe^{3+} sites, and of the formation of iron oxo-hydroxide clusters at high Fe contents, with the 480 nm band occurring due to *d-d* transitions of Fe_2O_3 clusters[36,39]. The spectrum of Fe-L-IMO, similar to that of Fe-1.4-IMO, is slightly shifted towards higher wavelengths and is more intense in the *d-d* transition range. Such results indicate that iron oxo-hydroxide cluster formation is favored by post-synthesis exchange, although Al^{3+}/Fe^{3+} IS also occurs.

The Tauc's plot in **Figure 4b** shows that IMO has a band gap $E_g = 4.9$ eV, in agreement with the calculated value (4.6 eV)[34]. Doping with Fe brings about a significant decrease of the band gap. With the Fe-0.70-IMO sample, where mostly IS Fe^{3+} species occur, E_g is 2.8 eV, indicating that Fe-doping has the effect of lowering the band gap since the sample is approaching semi-conductor behavior. With Fe-L-IMO, an even lower band gap is measured ($E_g = 2.4$ eV), although the presence of iron oxo-hydroxide clusters hampers a more precise determination of E_g in this sample.

The samples' behavior in water is investigated by means of ζ-potential measurements and adsorption of $AO7^-$ from an aqueous solution at pH = 6.8. Since IR spectra reported elsewhere[39] did not reveal relevant differences between IMO and Fe-0.70-IMO (due to the low Fe content), only the samples with mass fractions of 1.4% Fe were considered. The ζ-potential curve of IMO (**Figure 5a**) shows that it is positively charged at low pH values, with a point of zero charge (PZC) at pH = 9.8 (*i.e.,* very close to that of alumina)[44,45]. Fe-doped samples show a very similar behavior: the net difference in both surface charge and PZC among the samples is not relevant. As a whole, the samples are positively charged at low pH and negatively charged at high pH; therefore, all of them should be able to adsorb anions and cations above and below their PZC, respectively.

$AO7^-$ adsorption results are reported in **Figure 5b** as percentage of dye adsorbed as a function of time. The best performance is given by Fe-1.4-IMO, followed by IMO, indicating that the main process is an electrostatic attraction between $AO7^-$ anions and the positively-charged outer surfaces of the samples (the solution pH was 6.8).

However, some important differences are observed: Fe-1.4-IMO gives the best performance in terms of $AO7^-$ removal, with a steep increase in the dye adsorption in the very first minutes (accompanied by a pH drop, as reported in Ref. 39). The same occurs, to a minor extent, with Fe-0.70-IMO, because reaction (3) takes place:

$$Fe(OH)_2^+Al + AO7^- = FeAO7^- + Al\text{-}OH + H^+ \quad (3)$$

which implies the formation of $FeAO7^-$ adducts through a ligand displacement phenomenon, with N atoms of the dye coordinating IS Fe^{3+} sites.

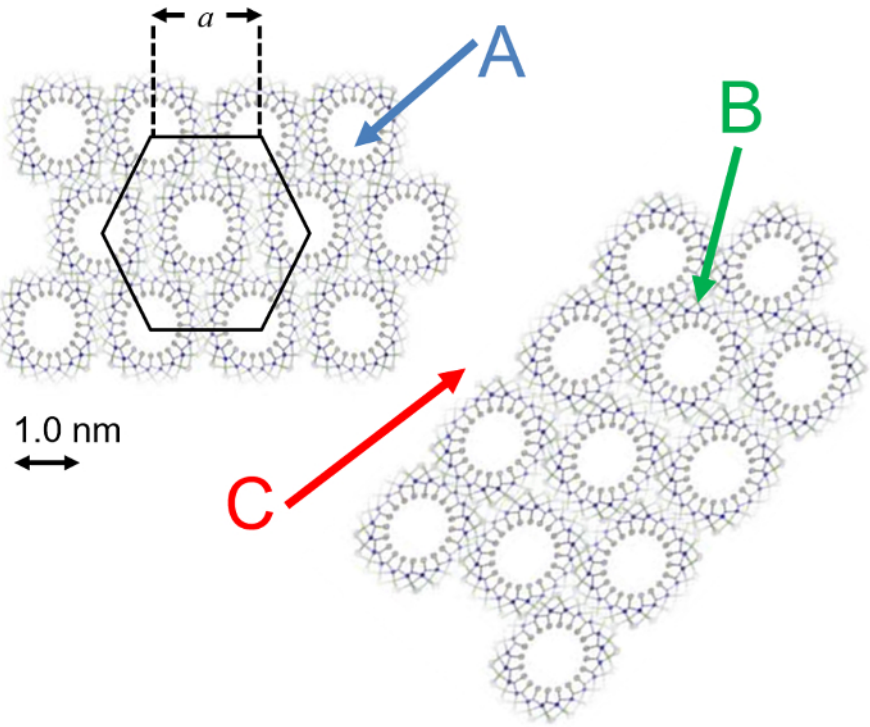

Figure 1. Representation of two bundles of IMO NTs in hexagonal packing. When occurring in powder form, IMO NTs are packed in bundles having nearly hexagonal symmetry. The cell parameter *a* evidenced in the figure corresponds to the center-to-center distance between two aligned NTs within a hexagonal bundle. Pores A, B, and C correspond to proper IMO nanopores (~1.0 nm wide), nanopores among three aligned NTs (~0.30-0.40 nm wide), and slit mesopores among bundles, respectively. Please click here to view a larger version of this figure.

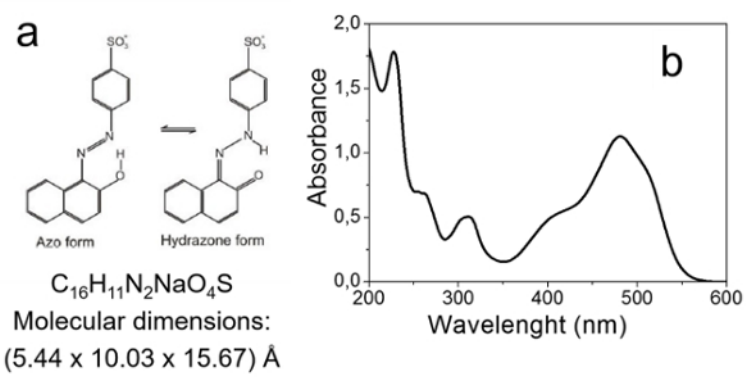

Figure 2. The azo-dye Acid Orange 7 in water: azo-hydrazone tautomerism and UV-Vis spectrum. Part (**a**) reports the chemical formula and molecular dimensions[42] of the dye along with its azo- and hydrazone forms, both present in water solution due to tautomerism. Part (**b**) reports the UV-Vis spectrum of the initial 0.67 mM solution of the dye used for the adsorption experiments[39]. Please click here to view a larger version of this figure.

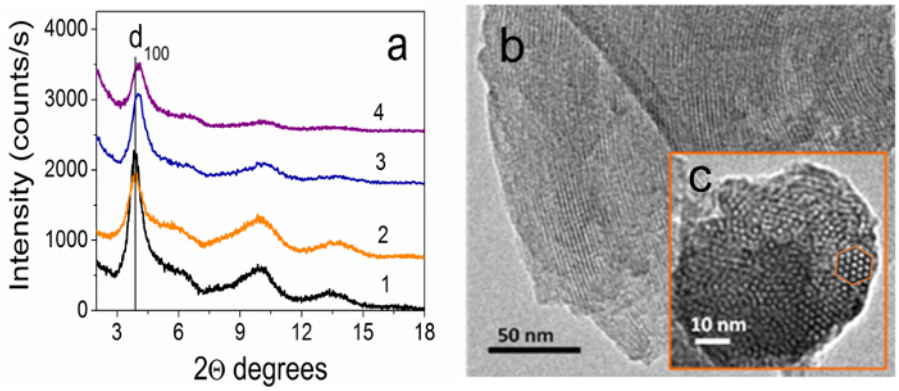

Figure 3. Textural characterization of the synthesized powder samples. Part (**a**) reports low-angle XRD patterns of IMO (curve 1), Fe-L-IMO (curve 2), Fe-0.70-IMO (curve 3), and Fe-1.4-IMO (curve 4). Parts (**b**) and (**c**) refer to sample Fe-0.70-IMO; a selected HRTEM micrograph of the powder sample is reported (**b**), along with a magnification of the frontal view of a bundle with NTs forming a hexagonal array (**c**). Please click here to view a larger version of this figure.

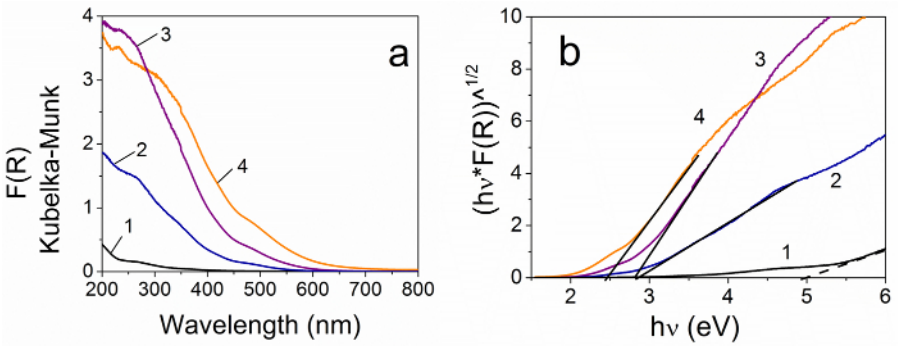

Figure 4. DR-UV-Vis spectroscopic characterization of the synthesized powder samples. Part (**a**) reports the DR-UV-Vis spectra of IMO (curve 1), Fe-0.70-IMO (curve 2), Fe-1.4-IMO (curve 3), and Fe-L-IMO (curve 4). Part (**b**) reports the corresponding Tauc's plots, from which the band gap values (E_g, eV) reported in **Table 1** were determined. Please click here to view a larger version of this figure.

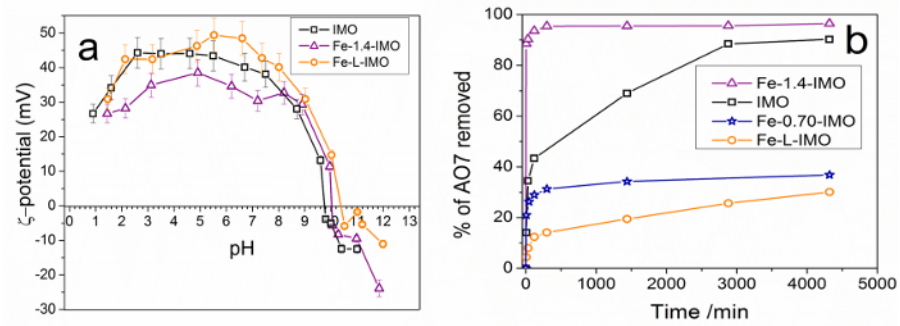

Figure 5. Measurements of the samples' surface charges and Acid Orange 7 adsorption experiments. Part (**a**) reports the ζ-potential curves of IMO (squares), Fe-1.4-IMO (triangles), and Fe-L-IMO (circles); error bars correspond to 10% of the measured value, according to previous works[38,39]. Part (**b**) reports the percentage of $AO7^-$ removed versus time for IMO (squares), Fe-0.70-IMO (stars), Fe-1.4-IMO (triangles), and Fe-L-IMO (circles). Please click here to view a larger version of this figure.

Sample	Fe, wt%	BET SSA (m^2 g^{-1})	Total Volume (cm^3 g^{-1})	Micropore Volume (cm^3 g^{-1})	d_{100} (nm ±0.01)	a (nm)	Band gap (eV)	PZC	$AO7^-$ removed
IMO	-	383	0.21	0.13	2.27	2.62	4.9	9.8	95%
Fe-L-IMO	1.4	400	0.27	0.13	2.27	2.62	2.4	10.0	30%
Fe-0.70-IMO	0.70	450	0.22	0.15	2.19	2.53	2.8	-	37%
Fe-1.4-IMO	1.4	455	0.22	0.14	2.17	2.51	2.8	10.4	96%

Table 1. Relevant properties of the samples, as determined by N_2 isotherms at -196 °C, XRD patterns, DR-UV-Vis spectroscopy, ζ-potential measurements, and adsorption experiments with $AO7^-$ water solutions.

Discussion

In order to be successful, the reported protocol has to be carefully followed, since formation of NTs strictly depends on the synthesis conditions. The following steps are critical: in steps 1.2 and 2.3, a slight excess of TEOS has to be used with respect to the Si/Al stoichiometry ratio (*i.e.,* TEOS:ATBS = 1.1:2). The excess of TEOS prevents the preferential formation of gibbsite ($Al(OH)_3$) and/or boehmite (AlOOH) phases[46,47].

Another crucial point is the fast hydrolysis of ATBS. To prevent this, a moisture-free environment is needed (*e.g.,* the dry room adopted in this work). In a dry environment, it is possible to measure the volumes of both TEOS and ATBS using graduated pipettes, avoiding ATBS hydrolysis that would lead to an unsuccessful synthesis.

Another crucial point is the dilution in step 1.6. At higher reagent concentrations, condensation of orthosilicic acid would hinder the formation of NTs.

During polymerization, the temperature has to be controlled carefully. The temperature of polymerization during step 1.7 should not exceed 100 °C. To the best of our knowledge, the optimum range of temperature for polymerization in order to obtain a high yield of pure NTs is 95-100 °C. At lower temperatures, the NT formation rate decreases, whereas at higher temperatures, other impurities (*e.g.,* aluminum oxides) form[48,49]. The use of a thermostat would be the best solution, but measuring the temperature close to the autoclave within the stove may be enough, as done in this work.

The main limitation of the synthesis protocol is that NTs do not form at mass fractions higher than 1.4% Fe, as reported in the literature by authors using a slightly different protocol[33]. This can be due to some structural strains induced by Fe in this type of structure. The second major limitation is the degree of Al^{3+}/Fe^{3+} IS that can be reached, corresponding to a maximum mass fraction of 1.0% Fe. It has to be noted, however, that the same was also observed with Fe-doped aluminogermanate NTs[37].

On the contrary, the occurrence of IS by post-synthesis loading is an interesting and encouraging result, likely related to the fact that Al(OH)Al groups on the outer surface of NTs are able to undergo ionic exchanges in solution, according to reaction (4):

$$[Al(OH)\,Al]_{(s)} + Fe(H_2O)_{6(aq)}^{3+} = [Fe(OH)\,Al]_{(s)} + Al(H_2O)_{6(aq)}^{3+} \quad (4)$$

This result is particularly relevant and shows that the proposed protocol has important outcomes, since it opens the possibility of changing the composition of the IMO outer surface by ionic exchange, thus avoiding more complicated procedures (*i.e.,* direct synthesis). As mentioned before, the synthesis of IMO requires several precautions in order to be successful, and the mere addition of another reagent-in the present case, $FeCl_3 \cdot 6H_2O$-will perturb the synthesis environment. It is indeed simpler to add the Fe precursor to an aqueous solution of preformed NTs, as done for the Fe-L-IMO sample. The same procedure could be extended to other cations with proper charges and radii, like Cr^{3+} and Ti^{3+}. In the case of Ti^{3+}, however, there could be some limitations due to the stability of the Ti^{3+} species and of its precursor.

Another important consequence of the successful doping procedure is the lowering of the IMO band gap. This result is particularly relevant if applications involving semiconductors are concerned, such as photocatalysis. Moreover, the presence of reactive Fe^{3+} surface species could be exploited in a photo-Fenton reaction for the removal of organic pollutants from water.

The formation of Fe(OH)Al groups as a consequence of Al^{3+}/Fe^{3+} IS provides Fe^{3+} sites that are accessible to species able to coordinate iron in water, as observed during the $AO7^-$ adsorption experiments reported here. This concept could be extended to the retention of other organic pollutants, making it possible to exploit the outer surface of NTs in adsorption processes involving not only mere electrostatic interaction, but ligand displacement as well.

The worst performance of Fe-L-IMO towards $AO7^-$ adsorption is ascribable to the occurrence of a larger fraction of clusters. After the addition of ammonia during loading, cluster formation mostly occurs on the outer surfaces of NTs, as confirmed by the pore volumes, reported in **Table 1**. There is an increase in the total pore volume by loading, whereas the micropore volume, amenable to type A pores, remains unchanged. IS Fe^{3+} sites likely acted as crystallization centers for iron oxo-hydroxide clusters. Due to cluster formation, IS Fe^{3+} sites were no more accessible to $AO7^-$ species, finally lowering the adsorption capacity of Fe-L-IMO towards the dye[39].

Disclosures

The authors have nothing to disclose.

Acknowledgements

The authors acknowledge Prof. Claudio Gerbaldi and Nerino Penazzi (Politecnico di Torino) for lending the dry room.

References

1. Ajayan, P.M. Nanotubes from carbon. *Chem. Rev.* **99** (7), 1787-1800 (1999).
2. Wada, S.I., Eto, A., Wada, K. Synthetic allophane and imogolite. *J. Soil. Sci.* **30** (2), 347-355 (1979).
3. Farmer, V.C., Adams, M.J., Fraser, A.R., Palmieri, F. Synthetic imogolite: properties, synthesis and possible applications. *Clay Miner.* **18** (4), 459-472 (1983).
4. Yoshinaga, N., Aomine, A. Imogolite in some ando soils. *Soil Sci. Plant Nutr.* **8** (3), 22-29 (1962).

5. Cradwick, P.D.G., Farmer, V.C., Russell, J.D., Wada, K., Yoshinaga, N. Imogolite, a Hydrated Aluminium Silicate of Tubular Structure. *Nature Phys. Sci.* **240**, 187-189 (1972).
6. Bonelli, B., *et al.* IR spectroscopic and catalytic characterization of the acidity of imogolite-based systems. *J. Catal.* **264** (2), 15-30 (2009).
7. Yang, H., Wang, C., Su, Z. Growth Mechanism of Synthetic Imogolite Nanotubes. *Chem. Mater.* **20** (13), 4484-4488 (2008).
8. Wada, S. Imogolite synthesis at 25 °C. *Clay Clay Miner.* **35** (5), 379-384 (1987).
9. Yucelen, G.I., *et al.* Shaping Single-Walled Metal Oxide Nanotubes from Precursors of Controlled Curvature. *Nano Lett.* **12**, 827-832 (2012).
10. Ackerman, W.C., *et al.* Gas/vapor adsorption in imogolite: a microporous tubular aluminosilicate. *Langmuir.* **9** (4), 1051-1057 (1993).
11. Wilson, M.A., Lee, G.S.H., Taylor, R.C. Benzene displacement on imogolite. *Clay Clay Miner.* **50** (3), 348-351 (2002).
12. Bonelli, B., Armandi, M., Garrone, E. Surface properties of alumino-silicate single-walled nanotubes of the imogolite type. *Phys. Chem. Chem. Phys.* **15 (32)**, 13381-13390 (2013).
13. Amara, M.S., *et al.* Hexagonalization of Aluminogermanate Imogolite Nanotubes Organized into Closed-Packed Bundles, *J. Phys. Chem. C.* **118**, 9299-9306 (2014).
14. MacKenzie, K.J., Bowden, M.E., Brown, J.W.M., Meinhold, R.H. Structural and thermal transformation of imogolite studied by ^{29}Si and ^{27}Al high-resolution solid-stated magnetic nuclear resonance. *Clay Clay Miner.* **37** (4), 317-324 (1989).
15. Kang, D. Y., *et al.* Dehydration, dehydroxylation, and rehydroxylation of single-walled aluminosilicate nanotubes. *ACS Nano.* 4, 4897-4907. (2010).
16. Zanzottera, C., *et al.* Thermal collapse of single-walled aluminosilicate nanotubes: transformation mechanisms and morphology of the resulting lamellar phases. *J. Phys. Chem. C.* **116** (13), 23577-23584 (2012).
17. Wada, S.I., Wada, K. Effects of Substitution of Germanium for Silicon in Imogolite. *Clay Clay Miner.* **30** (2), 123-128 (1982).
18. Thill, A., *et al.* Physico-Chemical Control over the Single-or Double-Wall Structure of Aluminogermanate Imogolite-like Nanotubes. *J. Am. Chem. Soc.* **134** (8), 3780-3786 (2012).
19. Mukherjee, S., Bartlow, V.M., Nair, S. Phenomenology of the growth of single-walled aluminosilicate and aluminogermanate nanotubes of precise dimensions. *Chem. Mater.* **17** (20), 4900-4909 (2005).
20. Kang, D.-Y., Zang. J., Jones, C.W., Nair, S. Single-Walled Aluminosilicate Nanotubes with Organic-Modified Interiors. *J. Phys. Chem. C.* **115** (15), 7676-7685 (2011).
21. Bottero, I. *et al.* Synthesis and characterization of hybrid organic/inorganic nanotubes of the imogolite type and their behaviour towards methane adsorption. *Phys. Chem. Chem. Phys.* **13** (2), 744-750 (2011).
22. Kang, D.-Y., *et al.* Direct Synthesis of Single-Walled Aminoaluminosilicate Nanotubes with Enhanced Molecular Adsorption Selectivity. *Nature Commun.* **5**, 3342 (2014).
23. Ma, W., Yah, M.O., Otsuka, H., Takahara, A. Application of imogolite clay nanotubes in organic-inorganic nanohybrid materials. *J. Mater. Chem.* **22** (24), 11887-11892 (2012).
24. Park, S. *et al.* Two-dimensional alignment of imogolite on a solid surface. *Chem. Commun.* 2917-2919 (2007).
25. Yamamoto, K., Otsuka, H., Wada, S., Takahara, A. Surface modification of aluminosilicate nanofiber "imogolite". *Chem. Lett.* **30**, 1162-1173 (2001).
26. Zanzottera, C., *et al.* Physico-chemical properties of imogolite nanotubes functionalized on both external and internal surfaces. *J. Phys. Chem. C.* **116** (13), 7499-7506 (2012).
27. Gustafsson, J.P. The surface chemistry of imogolite. *Clay Clay Miner.* **49** (1), 73-80 (2001).
28. Denaix, L.; Lamy, I.; Bottero, J.Y. Structure and affinity towards Cd^{2+}, Cu^{2+}, Pb^{2+} of synthetic colloidal amorphous aluminosilicates and their precursors. *Coll. Surf. A.* **158** (3), 315-325 (1999).
29. Clark, C.J., McBride, M.B. Cation and anion retention by natural and synthetic allophane and imogolite. *Clay Clay Miner.* **32** (4), 291-299 (1984).
30. Parfitt, R.L., Thomas, A.D., Atkinson, R.J., Smart, R. St.C. Adsorption of phosphate on imogolite. *Clay Clay Miner.* **22** (5-6), 455-456 (1974).
31. Arai, Y., McBeath, M., Bargar, J.R., Joye, J., Davis, J.A. Uranyl adsorption and surface speciation at the imogolite-water interface: Self-consistent spectroscopic and surface complexation models. *Geochim. Cosmochim. Acta.* **70** (10), 2492-2509 (2006).
32. Harsh, J.B., Traina, S.J., Boyle, J., Yang, Y. Adsorption of cations on imogolite and their effect on surface charge characteristics. *Clay Clay Miner.* **40** (6), 700-706 (1992).
33. Ookawa, M., Inoue, Y., Watanabe, M., Suzuki, M., Yamaguchi, T. Synthesis and characterization of Fe containing imogolite. *Clay Sci.* **12** (2), 280-284 (2006).
34. Alvarez-Ramìrez, F. First Principles Studies of Fe-Containing Aluminosilicate and Aluminogermanate Nanotubes. *J. Chem. Theory Comput.* **5** (12), 3224-3231 (2009).
35. Guimarães, L., Frenzel, J., Heine, T., Duarte, H.A., Seifert, G. Imogolite nanotubes: stability, electronic and mechanical properties. *ACS Nano.* **1** (4), 362-368 (2007).
36. Shafia, E. *et al.* Al/Fe isomorphic substitution versus Fe_2O_3 clusters formation in Fe-doped aluminosilicate nanotubes (imogolite). *J. Nanopar. Res.* **17** (8), 336 (2015).
37. Avellan, A. *et al.* Structural incorporation of iron into Ge-imogolite nanotubes: a promising step for innovative nanomaterials. *RSC Advances* **4** (91), 49827-49830 (2014).
38. Shafia, E., *et al.* Reactivity of bare and Fe-doped alumino-silicate nanotubes (imogolite) with H_2O_2 and the azo-dye Acid Orange 7. *Catal. Tod.* (2015).
39. Shafia, E., *et al.* Isomorphic substitution of aluminium by iron into single-walled alumino-silicate nanotubes: A physico-chemical insight into the structural and adsorption properties of Fe-doped imogolite. *Micropor. Mesopor. Mat.* **224**, 229-238 (2016).
40. Arancibia-Miranda, N., Acuña-Rougiera, C., Escudey, M., Tasca, F. *Nanomaterials.* **6** (2), 28 (2016).
41. Freyria, F.S., *et al.* Reactions of Acid Orange 7 with Iron Nanoparticles in Aqueous Solutions. *J. Phys. Chem. C.* **115** (49), 24143-24152 (2011).
42. Zhao, X., *et al.* Selective anion exchange with nanogated isoreticular positive metal-organic frameworks. *Nat. Commun.* **4,** 2344 (2013).
43. Bursill, L.A., Peng, J.L., Bourgeois, L.N. Imogolite: an aluminosilicate nanotube material. *Philos. Mag. A.* **80** (1), 105-117 (2000).
44. Rotoli, B.M. *et al.*Imogolite: An Aluminosilicate Nanotube Endowed with Low Cytotoxicity and Genotoxicity. *Chem. Res. Toxicol.* **27** (7), 1142-1154 (2014).
45. Shu, H.-Y., Chang, M.-C., Hu, H.-H., Chen, W.-H. Reduction of an azo dye acid black 24 solution using synthesized nanoscale zerovalent iron particles. *J. Colloid Interface Sci.* **314** (1), 89-97 (2007).

46. Farmer, V.C. Synthetic imogolite, a tubular hydroxylaluminum silicate. *International Clay Conference.* Amsterdam, Netherlands: Elsevier. (1978).
47. Farmer, V.C., Fraser, A.R., Tait, J.M. Synthesis of imogolite: a tubular aluminium silicate polymer. *J. Chem. Soc. Chem. Commun.* **13,** 462-463 (1977).
48. Violante, A., Huang, P.M. Formation mechanism of aluminum hydroxide polymorphs. *Clay Clay Miner.* **41** (5), 590-597 (1993).
49. Violante, P., Violante, A., Tait, J.M. Morphology of nordstrandite. *Clay Clay Miner.* **30** (6), 431-437 (1982).

